Soft Matter

Network Topologies Dictate Electromechanical Coupling in Liquid Metal-Elastomer Composites

Journal:	*Soft Matter*
Manuscript ID	SM-ART-06-2020-001094.R1
Article Type:	Paper
Date Submitted by the Author:	20-Jul-2020
Complete List of Authors:	Zolfaghari Moheb, Navid; Carnegie Mellon University, Civil Engineering Khandagale, Pratik ; Carnegie Mellon University Michael, Ford; Carnegie Mellon University, Dayal, Kaushik; Carnegie Mellon University, Majidi, Carmel; Carnegie Mellon University, Mechanical Engineering

Journal Name

ARTICLE TYPE

Cite this: DOI: 10.1039/xxxxxxxxxx

Network Topologies Dictate Electromechanical Coupling in Liquid Metal-Elastomer Composites†

Navid Zolfaghari,[a] Pratik Khandagale,[a] Michael J. Ford,[a] Kaushik Dayal,[b,c,d] and Carmel Majidi*[a,b,c]

Received Date
Accepted Date

DOI: 10.1039/xxxxxxxxxx

www.rsc.org/journalname

Elastomers embedded with micro- and nanoscale droplets of liquid metal (LM) alloys like eutectic gallium-indium (EGaIn) can exhibit unique combinations of elastic, thermal, and electrical properties that are difficult to achieve using rigid filler. For composites with sufficient concentrations of liquid metal, the LM droplets can form percolating networks that conduct electricity and deform with the surrounding elastomer as the composite is stretched. Surprisingly, experimental measurements performed on LM-embedded elastomers (LMEEs) show that the total electrical resistance of the composite increases only slightly even as the elastomer is stretched to several times its natural length. In contrast, Pouillet's Law would predict an exponential increase in resistance (Ω) with stretch (λ) due to the incompressibility of liquid metal and elastomer. In this manuscript, we perform a computational analysis to examine the unique electromechanical properties of conductive LMEE composites. Our analysis suggests that the gauge factor that quantifies electromechanical coupling (i.e. $\mathscr{G} = \{\Delta\Omega/\Omega_0\}/\lambda$) decreases with increasing tortuosity of the conductive pathways formed by the connected LM droplets. A dimensionless parameter for path tortuosity can be used to estimate $\mathscr{G}$ for statistically homogeneous LMEE composites. These results rationalize experimental observations and provide insight into the influence of liquid metal droplet assembly on the functionality of the composite.

Introduction

In order to be electrically conductive, soft elastomers are typically embedded with conductive filler particles that form a percolating network. These filler particles include structured carbon black[1–3], silver nanoflakes[4,5], or nickel microparticles[6,7]. Depending on the material composition, volume fractions, and filler distribution, such composites can achieve low electrical resistivity in their unstressed state. However, stretching can degrade the percolating network and lead to a dramatic increase in resistance when the elastomer is stretched to several times its natural length[6,8–10]. This undesirable electromechanical coupling arises from the significant mechanical mismatch between the rigid filler particles and surrounding elastomer matrix – as the elastomer stretches, particles that are in direct physical contact or in close enough proximity for electrical tunneling will separate and lose their electrical connectivity[11,12]. Although not an issue for low strain applications in which deformation is largely restricted to compression, twisting, or bending, loss of electrical connectivity due to an applied strain can be prohibitively limiting for applications in wearable computing, smart textiles, and soft robotics in which the conductive elastomer must maintain stable electrical resistance under significant stretch.

To address this limitation, researchers have developed a new class of conductive elastomers in which the rigid filler particles are replaced with micro- and nanoscale droplets of liquid metal (LM) alloys like eutectic gallium-indium (EGaIn)[13–15]. As with other conductive polymer composites, the LM droplets encapsulated within the elastomer can form a dense, percolating network that supports high electrical conductivity (Figure 1A). Because the droplets are in a liquid phase, they can deform with the surrounding elastomer and preserve the connectivity of the conductive network (Figure 1B). LM-embedded elastomer (LMEE) composites that are soft and electrically conductive have been demonstrated by embedding LM droplets in poly(dimethylsilxoane) (PDMS)[16–18], poly(ethylene-vinyl acetate)[19], polyacrylate[20], and liquid crystal elastomer[21]. In their natural (unstressed) state, these composites can have an electrical

[a] Department of Mechanical Engineering, Carnegie Mellon University, Pittsburgh, PA 15213.
[b] Department of Civil & Environmental Engineering, Carnegie Mellon University, Pittsburgh, PA 15213.
[c] Department of Materials Science & Engineering, Carnegie Mellon University, Pittsburgh, PA 15213.
[d] Center for Nonlinear Analysis, Carnegie Mellon University, Pittsburgh, PA 15213.
* Tel: (412) 268-2492; E-mail: cmajidi@andrew.cmu.edu
† Electronic Supplementary Information (ESI) available: [details of any supplementary information available should be included here]. See DOI: 10.1039/b000000x/

conductivity as large as $\sigma = 10^3$ S/cm (for reference, $\sigma = 3\times10^4$ and 6×10^5 S/cm for EGaIn and copper, respectively).[18] Moreover, referring to Figure 1C, the end-to-end electrical resistance (Ω) does not increase significantly with stretch (λ). This lack of dependence of resistance on strain is surprising since Pouillet's Law would predict a relative increase in electrical resistance of $\Delta\Omega/\Omega_0 = \lambda^2 - 1$ since both the liquid metal and surrounding elastomer are virtually incompressible. That the gauge factor $\mathscr{G} = \{\Delta\Omega/\Omega_0\}/\lambda$ is well below $\frac{\partial}{\partial\lambda}\Big|_{\lambda=1}\{\lambda^2 - 1\} = 2$ suggests that the volumetric conductivity σ *increases* with stretch. Compared with the piezoresistive effect in other conductive materials, this unusual electromechanical response implies "negative piezoresistivity" in which electrical resistivity decreases with positive tensile strain. Such an effect has not been commonly observed in other soft material systems.

For particle and droplet-filled conductive elastomers, electrical current passes through conductive pathways within a percolating network. For conductive composites with rigid particle fillers, electrical conductivity can be enabled by tunneling through the thin interface between two neighboring filler particles. In contrast, conductivity in LMEEs is primarily achieved through physical contact and coalescence of neighboring droplets within the elastomer. Several studies have examined electrical conductivity through electrical tunneling[22,22–25] based on calculations of the potential barriers at a tunnel junction[26,27]. Researchers have adapted these theories to examine the increase in resistance as the tunneling gap increases with tensile strain[11,12].

Compared to composites with rigid fillers, there has been relatively little theoretical study on the mechanical or electrical properties of LMEE composites. Analytical and computational studies of elastomers with liquid droplet inclusions have been limited to the following: modifications of Eshelby's theory of inclusions to examine mechanical stiffness[28–31], Maxwell-Garnett and Bruggeman effective medium approximations to study thermal conductivity and electrical permittivity[32,33], finite element analysis to model deformation of co-linear LM droplets[34], and use of the volume element method to show the effect of localized stresses on rupturing and coalescence of adjacent LM droplets[35]. In extending current computational approaches to analysis of LMEE electromchanical coupling, an important consideration is the uniform hydrostatic pressure within LM droplets and its influence on internal stress within the surrounding elastomer.

Here, we present a computational analysis that examines the electromechanical properties of conductive LMEE composites. As shown in Figure 1C, the model is capable of predicting theoretical bounds for electromechanical coupling that are in good agreement with experimental measurements. Our analysis suggests that $\mathscr{G}$ approaches zero as the tortuosity of the conductive pathways formed by the connected LM droplets increases. Path tortuosity can be represented with a dimensionless parameter γ that is used to predict $\mathscr{G}$ within a percolating network of connected LM droplets.

Electromechanical coupling in LMEE composites had previously been examined in Cohen and Bhattacharya[35], which provided a numerical model using a cubic representative volume element (RVE) method. Although their model didn't predict gauge factors for electromechanical coupling within the range of experimental measurements, they were able to demonstrate that local stresses induced around the droplets during mechanical deformation can cause the elastomer to rupture and allow adjacent LM droplets to coalesce. The current analysis goes further in theoretically validating the experimental measurements, with the goal of demonstrating that there exists a network of connected droplets that results in only a modest increase in electrical resistance Ω of the LMEE during stretch.

Using a finite element method (FEM), we model a variety of LM droplet microstructures that not only obey the mechanical deformation of the hyper-elastic matrix but also account for fluid flow. Based on this analysis, we are able to calculate the change in electrical power required to maintain a constant voltage droplet between the ends of the percolating network as it is stretched from its initial configuration:

$$\Delta P = \left(\frac{-V^2}{\Omega_0}\right)\left\{\frac{\Delta\Omega/\Omega_0}{\Delta\Omega/\Omega_0 + 1}\right\} \tag{1}$$

Finally, we provided a non-dimensional parameter γ that can quantify the change in normalized electrical resistance of the LMEE under deformation, which will provide guidance and rationalization to researchers engineering these composites and quantifying electromechanical coupling.

Computational Model

FEM-based computational modeling of the LMEE composites was performed in ANSYS V.19.2. The elastomer was treated as an incompressible Neo-Hookean solid with a strain energy density of

$$W = \frac{\mu}{2}(\bar{I}_1 - 3), \tag{2}$$

where μ is the initial shear modulus and $\bar{I}_1$ is the first deviatoric strain invariant. We assumed that the embedded LM droplets are in full contact with the surrounding elastomer and ignored any mechanical contributions from the nanometer-thin oxidization layer that typically forms at the LM-elastomer interface. Moreover, we ignored the presence of any air cavities or voids within the composite. The LM was treated as a homogeneous fluid with a viscosity μ_{Liq} and specific density ρ_{Liq}.

Droplet Geometry

In previous experimental studies, the shapes of droplets within LMEE composites were determined using optical imaging, electron microscopy, and X-ray computed tomography. In general, LM droplets can be spherical, ellipsoidal, or have irregular shapes, although most LMEEs are composed of LM inclusions with approximately spherical shape. For simplicity, we will limit analysis to composites in which the droplets are initially spherical prior to elastomer stretch and droplet elongation. Nonetheless, the FEM approach used here can be easily adapted to other microstructures in which the LM droplets have a non-spherical shape in the natural/unstressed state. Furthermore, we only modeled the deformation of droplets that are connected with their neighbors and along the path of electrical current flow. While other

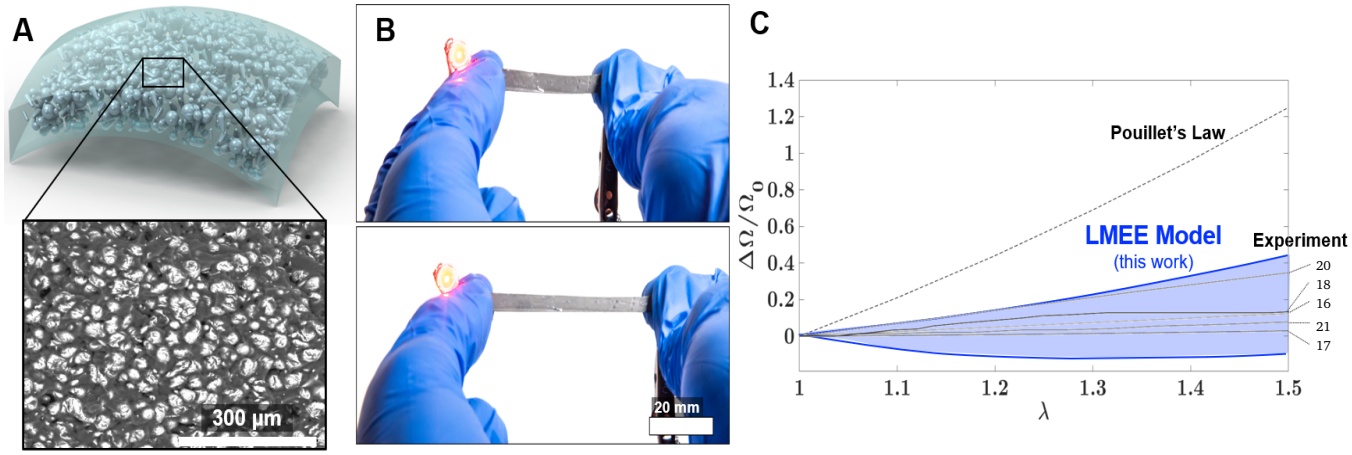

Fig. 1 (A) Schematic of LMEE morphology along with electron micrograph of LMEE cross section showing LM droplets (B) Photographs of LMEE powering LED while unstretched and stretched (C) Summary of the electromechanical coupling of reported LMEEs compared to Pouillet's Law and the model in this work. The blue shaded region that corresponds to our model represents the range of possible electromechanical coupling dependent on the geometry of the LM droplets.

droplets could have modest influence on the mechanical resistance to stretch, we assume that they will not contribute to the change in electrical resistance.

LMEEs are typically synthesized using shear mixing or ultrasonication, which typically results in LM droplets that are randomly distributed within the elastomer matrix. The droplets can be monodisperse or polydisperse and have a spatial distribution that is statistically uniform over volumes of interest. To simplify analysis, we examined small clusters of LM droplets that are well below the threshold of a RVE. Rather than aim for a statistically accurate representation of the LMEE microstructure, our goal was to demonstrate that there exist spatial arrangements of LM droplets within an elastomer that allow for the low, experimentally-measured values of electromechanical coupling presented in Figure 1C. We evaluated electromechanical coupling by examining seven different classes of spatial arrangements that were simple enough to parameterize but realistic and descriptive enough to capture the LM morphology and unique electromechanical properties of the composite. These arrangements can be co-planar or three-dimensional, with representative configurations for each class of geometries presented in Figure 2. In all the studied cases, the size of the volumetric element is much larger than the size of the droplets.

In this study, we ignore the role of surface oxide on the electrical or electromechanical properties of the droplet networks. In practice, however, the gallium-based LM alloys used in LMEEs are highly susceptible to oxide formation and this could influence the electrical resistance between contacting droplets. Such an influence could be especially pronounced for sub-micron LM droplets, for which the volume ratio of the insulating oxide could be significant. Moreover, we assume uniform droplet size and do not account for the influence of polydispersity on the electromechanical properties of the composite. However, polydispersity could be an important factor since it could lead to more complex network topologies that are outside the scope of the simple geometries examined here. Nonetheless, the computational methods adopted here could be generalized to model the presence of oxide layers as well as polydispersity of the LM suspensions.

Electrostatics

We used electrostatic field theory to assess the extent to which the electrical resistance Ω of an LMEE strip of natural length L_0 and cross-sectional area A_0 change with stretch $\lambda = L/L_0$ for the classes of geometries presented in Figure 2. These include the following: co-linear droplets with a center-to-center spacing ℓ (Fig. 2a); droplets arranged in a sawtooth pattern with spacing ℓ and angle θ (Fig. 2b); "horseshoe" arrangement with spacings $\{\ell_1, \ell_2\}$ and angles $\{\theta_1, \theta_2\}$ corresponding to the red and black segments shown in Fig. 2c; droplets in a rectangular arrangement (Fig. 2d); diamond formation with angle θ and center-to-center droplet spacing ℓ (Fig. 2e); 3D tetrahedron and pentahdron arrangements (Fig. 2f and (Fig. 2g, respectively).

In each case, we sought to determine the relative change in resistance as a function of λ, i.e. $\Delta\Omega/\Omega_0 = f(\lambda)$. Linearizing about $\lambda = 1$ yields an estimate of the gauge factor $\mathscr{G} = \lim_{\lambda\to 1}\{\Delta\Omega/\Omega_0\}/\lambda$. All of the results are compared with the idealized model for the change in electrical resistance for a homogenous and incompressible elastic solid:

$$\frac{\Delta\Omega}{\Omega_0} = \lambda^2 - 1\,, \tag{3}$$

which derives from Pouillet's Law, i.e. $\Omega = \rho L/A$ where ρ is the volumetric resistivity of the conductor. As shown in Figure **??** of the Supporting Information, this prediction is in exact agreement with predictions obtained when we perform FEM simulations for a prismatic cylindrical channel of liquid metal within a Neo-Hookean solid. In the following section, we report electromechanical coupling for elastomers embedded with the LM droplet geometries shown in Figure 2.

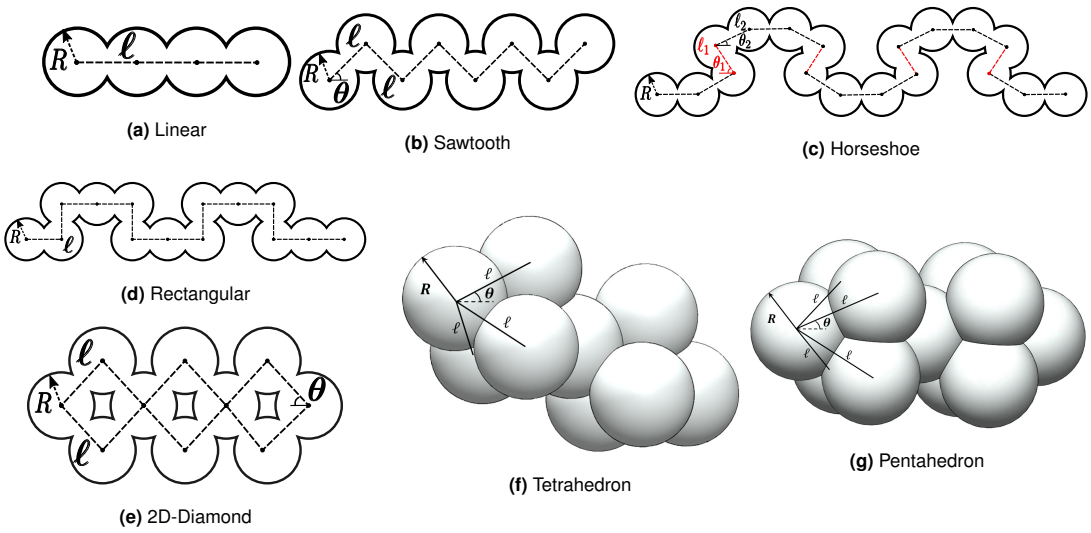

Fig. 2 Illustrations of different interconnectivity of the LM droplets in LMEE used in this study. The geometric parameters that were modified to study their influence on electromechanical coupling are shown, where R is the radius of the droplet, ℓ is the center-to-center distance between droplets, and θ is the angle of the connecting lines from horizontal.

Results & Discussion

Using the computational method described in the previous section, we obtain plots of $\Delta\Omega/\Omega_0$ versus λ for the selected class of geometries. For each type of spatial arrangement, electromechanical coupling is influenced by a variety of geometric parameters, including the droplet radius R and spacing ℓ. For the "horseshoe-like" serpentine patterns in Figure 2c, we define an additional geometric parameter γ that is associated with the tortuosity of the connected path.

Linear Configuration

As shown in Figure 2a, a linear pattern for liquid metal inclusions is defined as a sequence of spherical droplets of identical radius that are partially overlapped by a length $2R-\ell$. The key parameter that defines this geometry is the normalized spacing $k=\ell/R$, where ℓ is defined as the center-to-center distance between two adjacent spherical droplets. Figure 3 indicates the change of the effective electrical resistance ($\Delta\Omega/\Omega_0$) versus uniaxial stretching of the sample (λ) for different values of k ($k\in\{1.2,1.5,1.7,1.9\}$).

Reducing k will retrieve the solution for a cylindrical channel inside the elastomer, which corresponds to the algebraic expression derived from Pouillet's Law. Increasing k will cause $\Delta\Omega/\Omega_0$ at a given λ to decrease. Specifically, spacing the droplets farther apart will lead to a more narrow opening for liquid to flow between droplets. The FEM simulation suggests that stretching the elastomer will induce hydrostatic pressure that will force fluid to flow into this narrow opening and cause it to enlarge. For this reason, the increase in resistance with stretch is not as great as it is for a prismatic channel. Nonetheless, the gauge factor for these geometries is significantly higher than it is for the experimental measurements plotted in Figure 1C.

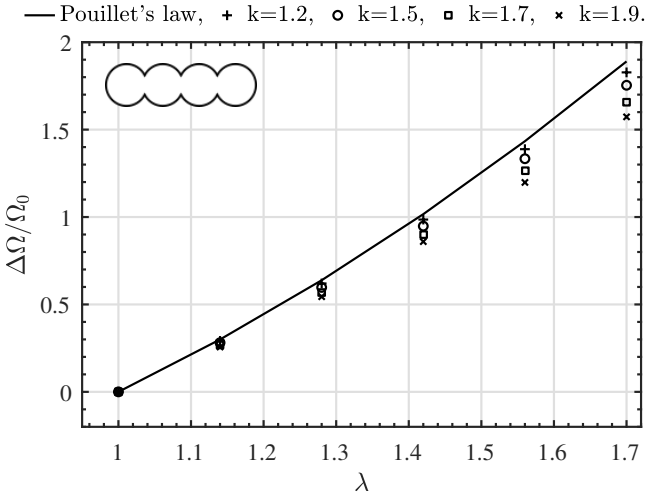

Fig. 3 Normalized change in electrical resistance as a function of strain for linear patterns of LM droplets with different values of k. Pouillet's law is shown for reference.

Sawtooth Configuration

Next, we consider the "sawtooth" pattern shown in Fig 2b. Here, the key parameters that define the geometry are the normalized spacing $k=\ell/R$ and sawtooth angle θ. Fig 4a shows the change of the effective electrical resistance for different configurations under loading. Compared to the linear configuration, the LM droplets arranged in a sawtooth configuration can exhibit significantly less electromechanical coupling, with $\mathscr{G}\approx 1$ in the case of $k=1.7$ and $\theta=40^{\circ}$.

As with the linear case, we see that increasing k will lead to a more narrow connection between adjacent droplets and a corresponding reduction in electromechanical coupling. We observe that increasing the angle θ can lead to an even more pronounced reduction in $\mathscr{G}$. Figures 4b and 4c compare two cases with the same k but different values of θ, where the total current density

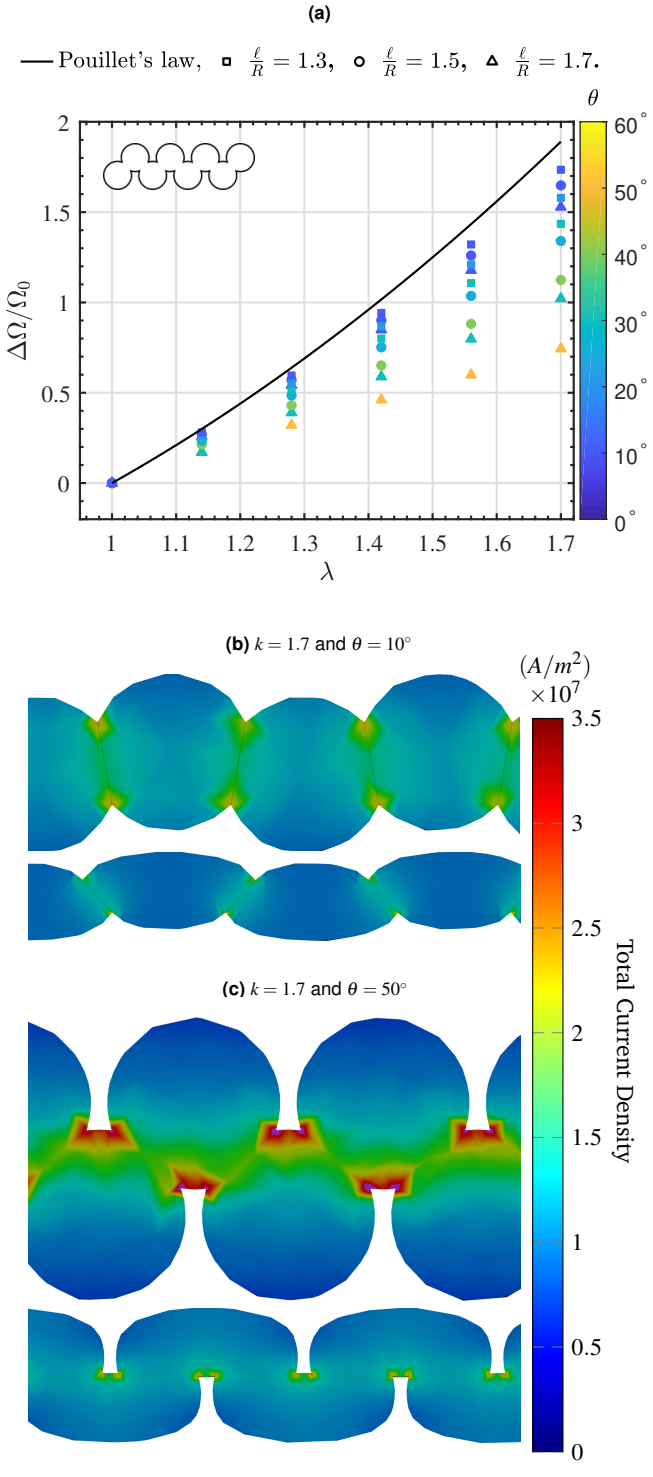

Fig. 4 (a) Normalized change in electrical resistance as a function of strain for sawtooth patterns of LM droplets with different geometric parameters. Pouillet's law is shown for reference. The major parameters that define the sawtooth configuration are ℓ/R and θ (see Figure 2b). (b,c) FEM comparison of the current density in two sawtooth patterns before (top) and after (bottom) an imposed strain. Both patterns have the same $k = \ell/R$ value but different angles of connectivity. In this figure the color map represent the total current density in the liquid metal.

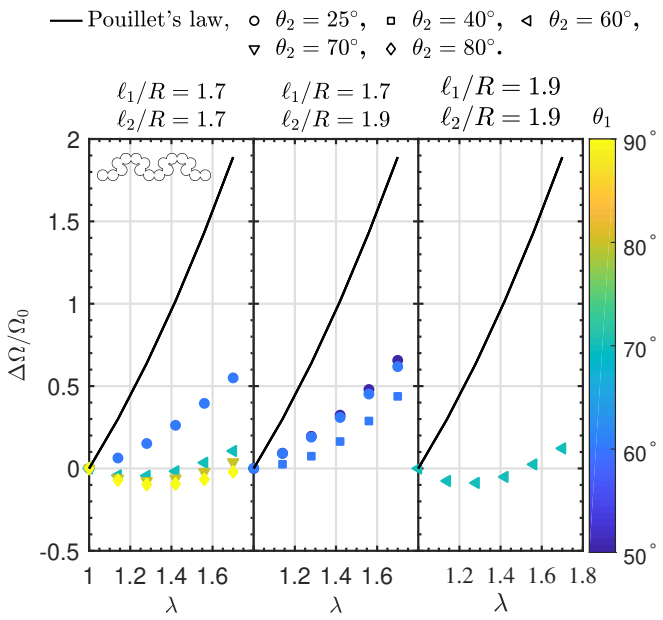

Fig. 5 Normalized change in electrical resistance as a function of strain for horseshoe patterns with different geometrical configurations. The main parameters that define the horseshoe patterns are ℓ_1/R, ℓ_2/R, θ_1 and θ_2 (see Figure 2c).

was monitored during stretching. As suggested by the FEM simulations, increasing the angle θ will cause the overlapped regions of the droplets to align with the direction of elongation. This alignment can reduce electrical resistance since after stretching the sample, the interfacial area between droplets increases rather than decreases, providing a larger opening for the electrical current to pass through (see Figure 4c). In this way, the current density along the pathway for the deformed solid in Fig 4b is higher than that shown in Fig 4c. Hence, we postulate that increasing the angle θ can decrease the normalized electrical resistance during strain.

Horseshoe Configuration

Referring to Figure 2c, LM droplets arranged in a "horseshoe" configuration can be parameterized by a series of center-to-center spacings ℓ_i and angles θ_i. In general, the index i is defined as $i \in \{1,...,N\}$ where N corresponds to the number of different pairs of segment lengths and angles defined along the path of the horseshoe geometry. Here, we find that two pairs of parameters (i.e. $i \in \{1,2\}$) are sufficient for achieving a spectrum of electromechanical properties that cover the behaviors that are measured experimentally during the strain. As before, each droplet was assumed to be a sphere of radius R and $k_i = \ell_i/R$ was defined as the ratio of the spacing of the spheres to their radius. For $N = 2$, we define ℓ_1 and ℓ_2 as the center-to-center spacing between droplets as shown by the red and black lines, respectively, in Figure 2c. Likewise, there are two different angles of θ_1 and θ_2 that define the tortuosity of the pattern.

Figs. 5 and 6 summarize the results for this class of geometries. Similar to the sawtooth configuration, we observe that increasing the values of θ_1 and θ_2 leads to a reduction in electrome-

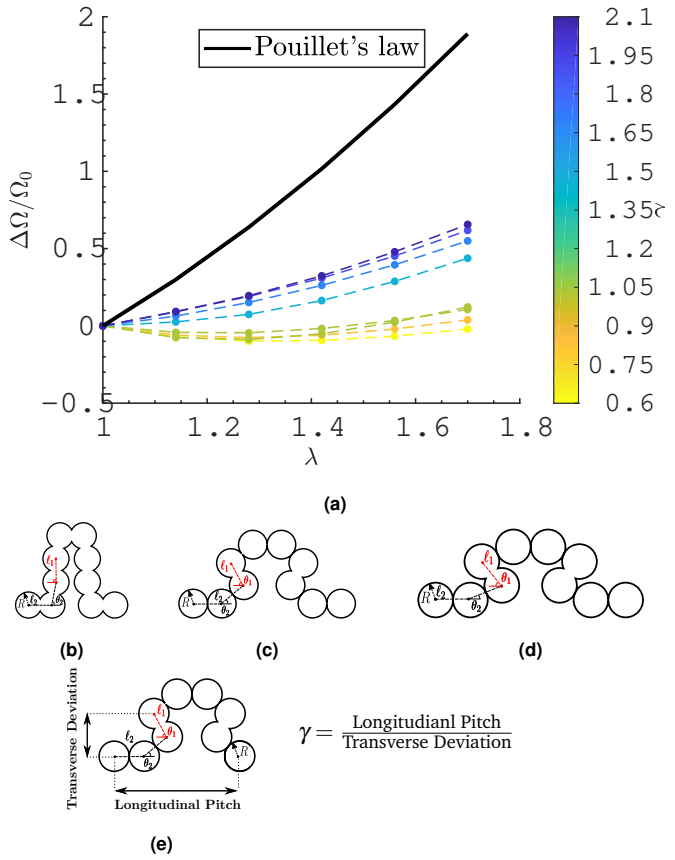

Fig. 6 a) Normalized change in electrical resistance as a function of strain for horseshoe patterns with different values of the tortuosity parameter. Schematics of droplet configuration for different tortuosity parameters: (γ). b) $\ell_1/R = \ell_2/R = 1.7, \theta_1 = 90°, \theta_2 = 80°$ and $\gamma = 0.68$. c) $\ell_1/R = 1.7, \ell_2/R = 1.9, \theta_1 = 60°, \theta_2 = 40°$ and $\gamma = 1.47$.d) $\ell_1/R = 1.7, \ell_2/R = 1.9, \theta_1 = 50°, \theta_2 = 25°$ and $\gamma = 2.02$. e) Definition of tortuosity parameter γ based on longitudinal pitch and transverse deviation.

chanical coupling (i.e. decrease in $\mathscr{G}$). This reduction implies that orienting portions of the LM connection chain in the direction perpendicular to elongation will result in decreased normalized electrical resistance when the LMEE composite is stretched. Moreover, increasing the value of k_1/k_2 for $\theta_1, \theta_2 \leq 90°$ can increase the resistance drop and vice versa. This observation may support the hypothesis that increasing the tortuosity of the pattern in the oblique direction from its stretching orientation can lower the change of the electrical resistance of the sample.

In order to further explore the influence of k_i and θ_i on $\mathscr{G}$, we defined the following dimensionless tortuosity parameter

$$\gamma = \frac{-\ell_1 cos(\theta_1) + 2\ell_2 cos(\theta_2) + \ell_2}{\ell_1 sin(\theta_1) + \ell_2 sin(\theta_2)}$$

where the numerator of γ is the longitudinal pitch of the pattern while the denominator is the transverse deviation. Increasing the tortuosity parameter caused an increase in electromechanical coupling (Fig 6). The variable γ is a scale-invariant parameter that describes the horseshoe-like configuration. Based on the definition of γ, letting $\theta_1 = 180°$ and $\theta_2 = 0°$ will cause γ to approach infinity. In this limiting case, the electromechanical response approaches that of the linear pattern shown in Figure 2a, which is similar to the case of a prismatic cylindrical channel ($\Delta\Omega/\Omega_0 = \lambda^2 - 1$). As shown in the figure, configurations with $\gamma < 2$ exhibit only modest electromechanical coupling relative to Pouillet's Law and have gauge factors that are similar to what has been measured experimentally. Interestingly, when $\gamma < 1$, the resistance initially decreases with strain (i.e. $\mathscr{G} < 0$). This behavior has been anecdotally observed in experimental measurements of LMEE composites[16,18] and could guide future work in controlled assembly of LM particles where control of electromechanical coupling is desired.

Other Patterns

Beside the three classes of configurations described above, we also studied the following LM arrangements: the 2D diamond pattern shown in Fig 2e, the rectangular pattern in Fig 2d, the 3D tetrahedral pattern in Fig 2f, and the pentahedral pattern in Fig 2g. Results for these alternative geometries are presented in Fig 7 alongside the 2D patterns discussed previously. As expected from our previous analyses, $\mathscr{G}$ is largest for the more linear patterns and is smallest for configurations with more meandering pathways.

Interestingly, the 2D diamond, which is comprised of two sawtooth patterns that are mirrored along the axis of stretch exhibits greater electromechanical coupling than the sawtooth arrangement of Figure 2b. This increase in electromechanical coupling is because the hydrostatic pressure in the diamond configuration is distributed more in 3D compared to a 2D configuration and so less fluid flows into the narrow connections between the adjacent droplets when the composite is stretched. Therefore, the interfacial area that form connections between LM droplets does not increase as much as it does in the sawtooth configuration, where the hydrostatic pressure is greater during strain. Similarly, the tetrahedral and pentahedral arrangements exhibit increased elec-

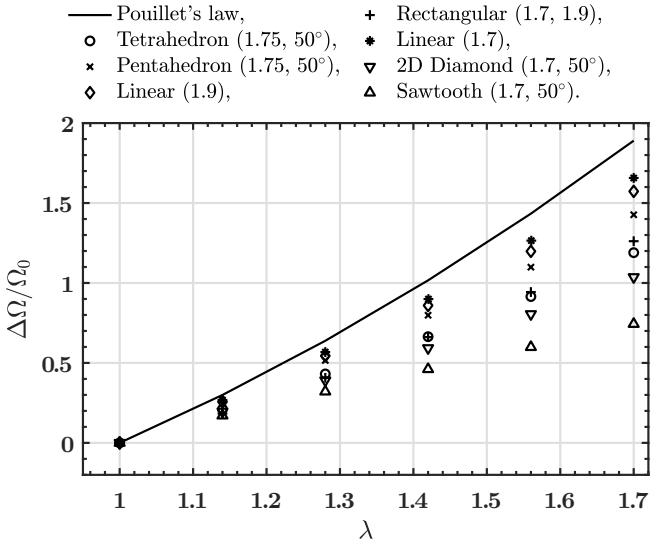

Fig. 7 The change of normalized electrical resistance for different microstructural patterns for LM fillers.

tromechanical coupling relative to the 2D diamond case. In these 3D configurations, the liquid metal is less confined and can flow in more directions during mechanical deformation.

Together, these results suggest that the low electromechanical coupling that has been observed in experimental measurements is most likely driven by the tortuosity of the meandering conductive pathways within the liquid metal's percolating network. While the hydrostatic pressure and its effect on the interfacial area between adjacent LM droplets subjected to strain also appear to have a role, it is not sufficient to account for the virtual absence of electromechanical coupling ($\mathscr{G} \approx 0$) that has been experimentally observed.

Comparison with Experiment

The model that we proposed here is capable of explaining the range of experimentally observed electromechanical coupling values for LMEE composites in the literature. By restricting ourselves to the various geometric classes and parameterizations introduced in Figure 2, we were able to generate theoretical predictions for electromechanical coupling that conform to experimental measurements. As shown in Fig 8, the sawtooth geometry matches well with the higher electromechanical coupling observed for an open-foam LM-PDMS sponge[36]. In contrast, theoretical results for the horseshoe geometry appear to be in reasonable agreement with measurements obtained for LMEE composites with fully enclosed LM inclusions. In all cases, comparison is done by fitting the geometric parameters. In this sense, the theory is intended to show that the low electromechanical coupling that has been observed experimentally is consistent with predictions for LM microstructures that are within the space of admissible geometries.

Conclusions

In contrast to other conductive elastomers, LMEE composites exhibit only modest electromechanical coupling – i.e. the end-to-end electrical resistance does not increase significantly with stretch. While demonstrated experimentally by several research groups, this surprising property and the influence of various LM morphologies had not been fully examined using analytic or computational techniques. In this study, we perform simulations in FEM that show that electromechanical coupling is influenced by LM droplet spacing and shape of the connected pathway. In the simplified case of serpentine paths with horseshoe-shaped turns, we observe electromechanical properties that are similar to what is observed experimentally. For other classes of 2D and 3D droplet arrangements, the gauge factor is below the value predicted for a homogeneous, incompressible conductive material but larger than what has been experimentally measured in LMEE composites produced using shear mixing techniques. These results may provide guidance if control of assembly of LM droplets could be achieved, where the control of the arrangement into prescribed shapes could be used to control the electromechanical coupling.

By comparing strain response for seven classes of geometries, we find two principle contributions to the reduction in electromechanical coupling. One contribution is the pressure-controlled opening of the narrow, neck-like connection that forms between connected droplets. These narrow connections are a significant source of electrical resistance when the composite is in its unstressed state. When the LMEE is stretched, fluid will flow into the neck and cause an expansion that will reduce the electrical resistance between the contacting droplets. However, this reduction in resistance doesn't fully compensate for the increase in resistance that arises from elongation and narrowing of the droplets themselves. Instead, our FEM results suggest that the primary source of reduced electromechanical coupling arises from the serpentine arrangement of the droplets. Stretching will cause these meandering paths to stretch out but will not significantly alter their length or average cross-sectional area, thereby preserving their end-to-end electrical resistance. Such coupling is captured using a dimensionless tortuosity parameter γ that corresponds to how straight the conductive pathways are within the percolating LM network.

In this study we have not examined the influence of LM volume fraction of the entire LMEE composite on its electromechanical properties. Instead, we examine the electromechanical coupling of a single chain of connected LM droplets. Nonetheless, it is possible that LM volume fraction could have an influence on the types of network topologies that are more statistically likely to occur within the composite. Such an analysis could be an interesting topic for future study. Moreover, further computation will be required to extend the simplified analysis presented here to more complex 3D geometries that more accurately represent the statistically uniform but random distribution of LM droplets within a LMEE composite. Such an analysis should account for stochasticity in both spatial distribution of droplets as well as in size, shape, and orientation of LM droplet. Nonetheless, the current analysis succeeds in demonstrating LM microstructures with theoretical electromechanical properties that are consistent with what are observed experimentally. The analysis confirms that experimental measurements showing the constant electrical resistance of LMEE composites are consistent with foundational principles

of electrostatics, hyperelasticity, and fluid-structure interaction.

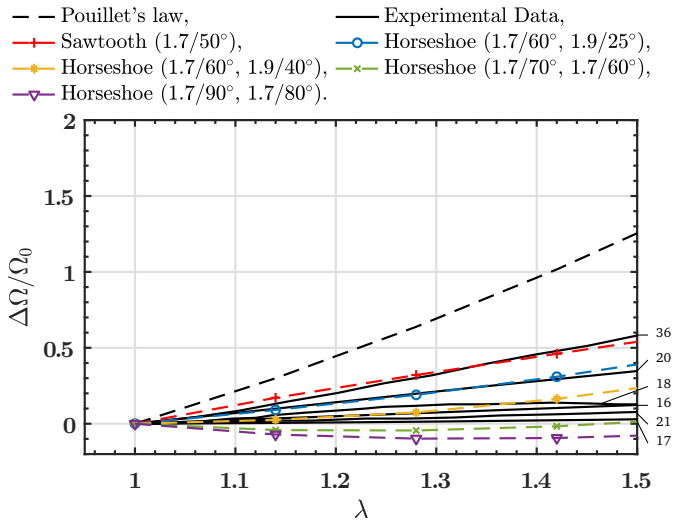

Fig. 8 Comparison of electro-mechanical coupling response of the LMEE observed experimentally in the literature with models generated in this work.

Acknowledgments

This research was supported by the Air Force Office of Scientific Research (AFOSR) Multidisciplinary University Research Initiative (FA9550-18-1-0566; Program Manager: K. Goretta). KD acknowledges ARO (W911NF-17-1-0084), ONR (N00014-18-1-2528), AFOSR (MURI FA9550-18-1-0095) and NSF (1635407). The authors would also like to acknowledge use of the Materials Characterization Facility at Carnegie Mellon University under grant # MCF- 677785.

Notes and references

1 B. Boonstra and E. M. Dannenberg, *Industrial & Engineering Chemistry*, 1954, **46**, 218–227.

2 J.-C. Huang, *Advances in Polymer Technology: Journal of the Polymer Processing Institute*, 2002, **21**, 299–313.

3 S. Khan and L. Lorenzelli, *Smart Materials and Structures*, 2017, **26**, 083001.

4 X. Niu, S. Peng, L. Liu, W. Wen and P. Sheng, *Advanced Materials*, 2007, **19**, 2682–2686.

5 N. Matsuhisa, M. Kaltenbrunner, T. Yokota, H. Jinno, K. Kuribara, T. Sekitani and T. Someya, *Nature communications*, 2015, **6**, 7461.

6 M. Park, J. Park and U. Jeong, *Nano Today*, 2014, **9**, 244–260.

7 T. Lu, J. Wissman and C. Majidi, *ACS applied materials & interfaces*, 2015, **7**, 26923–26929.

8 C. Pan, Y. Ohm, J. Wang, M. J. Ford, K. Kumar, S. Kumar and C. Majidi, *ACS applied materials & interfaces*, 2019, **11**, 42561–42570.

9 S. P. Lacour, S. Wagner, Z. Huang and Z. Suo, *Applied physics letters*, 2003, **82**, 2404–2406.

10 T. H. Ware, J. S. Biggins, A. F. Shick, M. Warner and T. J. White, *Nature communications*, 2016, **7**, 1–7.

11 M. Knite, V. Teteris, A. Kiploka and J. Kaupuzs, *Sensors and Actuators A: Physical*, 2004, **110**, 142–149.

12 W. Luheng, D. Tianhuai and W. Peng, *Carbon*, 2009, **47**, 3151–3157.

13 M. D. Dickey, R. C. Chiechi, R. J. Larsen, E. A. Weiss, D. A. Weitz and G. M. Whitesides, *Advanced Functional Materials*, 2008, **18**, 1097–1104.

14 N. Kazem, T. Hellebrekers and C. Majidi, *Advanced Materials*, 2017, **29**, 1605985.

15 M. D. Dickey, *Advanced Materials*, 2017, **29**, 1606425.

16 A. Fassler and C. Majidi, *Advanced Materials*, 2015, **27**, 1928–1932.

17 Z. Yu, J. Shang, X. Niu, Y. Liu, G. Liu, P. Dhanapal, Y. Zheng, H. Yang, Y. Wu, Y. Zhou *et al.*, *Advanced Electronic Materials*, 2018, **4**, 1800137.

18 E. J. Markvicka, M. D. Bartlett, X. Huang and C. Majidi, *Nature materials*, 2018, **17**, 618–624.

19 J. Wang, G. Cai, S. Li, D. Gao, J. Xiong and P. S. Lee, *Advanced Materials*, 2018, **30**, 1706157.

20 C. J. Thrasher, Z. J. Farrell, N. J. Morris, C. L. Willey and C. E. Tabor, *Advanced Materials*, 2019, **31**, 1903864.

21 M. J. Ford, C. P. Ambulo, T. A. Kent, E. J. Markvicka, C. Pan, J. Malen, T. H. Ware and C. Majidi, *Proceedings of the National Academy of Sciences*, 2019, **116**, 21438–21444.

22 Y. Yu, G. Song and L. Sun, *Journal of Applied Physics*, 2010, **108**, 084319.

23 W. Bao, S. Meguid, Z. Zhu and G. Weng, *Journal of Applied Physics*, 2012, **111**, 093726.

24 M. H. Wichmann, S. T. Buschhorn, J. Gehrmann and K. Schulte, *Physical Review B*, 2009, **80**, 245437.

25 X.-W. Zhang, Y. Pan, Q. Zheng and X.-S. Yi, *Journal of Polymer Science part B: polymer physics*, 2000, **38**, 2739–2749.

26 R. Holm, *Journal of Applied Physics*, 1951, **22**, 569–574.

27 J. G. Simmons, *Journal of applied physics*, 1963, **34**, 1793–1803.

28 R. W. Style, J. S. Wettlaufer and E. R. Dufresne, *Soft matter*, 2015, **11**, 672–679.

29 P. S. Owuor, S. Hiremath, A. C. Chipara, R. Vajtai, J. Lou, D. R. Mahapatra, C. S. Tiwary and P. M. Ajayan, *Advanced Materials Interfaces*, 2017, **4**, 1700240.

30 P. Sharma, S. Ganti and N. Bhate, *Applied Physics Letters*, 2003, **82**, 535–537.

31 S. Krichen, L. Liu and P. Sharma, *Journal of the Mechanics and Physics of Solids*, 2019, **127**, 332–357.

32 M. D. Bartlett, A. Fassler, N. Kazem, E. J. Markvicka, P. Mandal and C. Majidi, *Advanced Materials*, 2016, **28**, 3726–3731.

33 M. D. Bartlett, N. Kazem, M. J. Powell-Palm, X. Huang, W. Sun, J. A. Malen and C. Majidi, *Proceedings of the National Academy of Sciences*, 2017, **114**, 2143–2148.

34 X. Yi, Z. Yu, X. Niu, J. Shang, G. Mao, T. Yin, H. Yang, W. Xue, P. Dhanapal, S. Qu *et al.*, *Advanced Electronic Materials*, 2019, **5**, 1800655.

35 N. Cohen and K. Bhattacharya, *International Journal of Non-Linear Mechanics*, 2019, **108**, 81–86.
36 S. Liang, Y. Li, Y. Chen, J. Yang, T. Zhu, D. Zhu, C. He, Y. Liu, S. Handschuh-Wang and X. Zhou, *Journal of Materials Chemistry C*, 2017, **5**, 1586–1590.